

Spatial Bayesian Variable Selection Models on Functional Magnetic Resonance Imaging Time-Series Data

Kuo-Jung Lee ^{*} and Galin L. Jones [†] and Brian S. Caffo [‡] and Susan S. Bassett [§]

Abstract. A common objective of fMRI (functional magnetic resonance imaging) studies is to determine subject-specific areas of increased blood oxygenation level dependent (BOLD) signal contrast in response to a stimulus or task, and hence to infer regional neuronal activity. We posit and investigate a Bayesian approach that incorporates spatial and temporal dependence and allows for the task-related change in the BOLD signal to change dynamically over the scanning session. In this way, our model accounts for potential learning effects in addition to other mechanisms of temporal drift in task-related signals. We study the properties of the model through its performance on simulated and real data sets.

Keywords: Bayesian variable selection, fMRI, Ising distribution, Markov chain Monte Carlo

1 Introduction

Functional neuroimaging experiments typically aim to uncover localized regions in the brain which activate during a task, describe the networks required for a particular brain function or assess physical characteristics that result from disease or trauma. Our focus is on functional magnetic resonance imaging (fMRI) techniques to detect task-related neuronal activation. However, neuronal activation occurs too quickly to be observed directly in fMRI experiments. Despite this, the principle of neurovascular coupling (that is, local neuronal activation is related to changes in cerebral blood flow) allows indirect observation of activation via the blood oxygenation level dependent (BOLD) signal contrast.

The typical single-subject fMRI experiment is conceptually straightforward. A subject in an MRI scanner performs a task in response to a stimulus while three-dimensional images of the subject's brain are captured every 2-3 seconds. However, the data has a complicated structure. Imagine that the image is divided into a regular grid of volume elements, or *voxels*. The BOLD signal is observed at each voxel at each time point resulting in an enormous amount of data (possibly as many as 40 million observations) exhibiting both spatial and temporal dependence. Moreover, the data tend to be noisy and have a weak signal. Hence accurate and powerful models of single-subject task-related activation would be useful in developing effective imaging biomarkers. Unfortunately

^{*}Department of Statistics, National Cheng Kung University, Taiwan kjlee@stat.ncku.edu.tw

[†]School of Statistics, University of Minnesota, Minneapolis, MN, U.S.A. galin@stat.umn.edu

[‡]Department of Biostatistics, Johns Hopkins University, Baltimore, MD, U.S.A. bcaffo@jhsp.hopkins.edu

[§]Department of Psychiatry, Johns Hopkins University, Baltimore, MD, U.S.A. sbassett@jhmi.edu

there are few, if any, off-the-shelf methods for constructing sensible, computationally feasible statistical models in this situation. Indeed, Lindquist (2008) considered only non-Bayesian approaches and concluded

The size and complexity of the data make it difficult to create a full statistical model for describing its behavior, and a number of shortcuts are required to balance computational feasibility with model efficiency.

In fact, standard non-Bayesian approaches (e.g. Friston et al. 1994; Chen et al. 2009; Nichols and Holmes 2002; Worsley et al. 1992; Worsley 2003) do not produce a full model. However, many of these methods are computationally efficient.

The Bayesian paradigm provides an attractive inferential framework within which to develop models directly incorporating the physical characteristics of the experiment. Hence Bayesian methods in neuroimaging have received a fair amount of recent attention, see e.g. Bowman et al. (2008), Caffo et al. (2011), Genovese (2000), Goldsmith et al. (2014), Smith et al. (2003), Smith and Fahrmeir (2007), Woolrich et al. (2004), and Xia et al. (2009). We use Bayesian variable selection methodology to detect task-specific changes in the BOLD signal. The basic idea is now described while the details are given in Section 2. For voxel $v = 1, \dots, N$ let $y_{v,i}$ be the BOLD image intensity and $x_{v,i}$ the transformed stimulus at time $i = 1, \dots, T_v$. Then we assume a linear model

$$y_{v,i} = z_i^T a_v + x_{v,i} \beta_v + \varepsilon_{v,i} .$$

The baseline trend $z_i^T a_v$ is a linear combination of basis functions to remove low-frequency stimulus-independent effects. Next, β_v is interpreted as the activation amplitude while $x_{v,i}$ is the convolution of a stimulus function s and a parametric hemodynamic response function (HRF) h . It is necessary to transform the input functions since for a short-duration stimulus the BOLD response increases above baseline about 2 seconds after the onset of neuronal activity, peaking at about 5-8 seconds and falling below baseline (the undershoot) for about 10 seconds (Aguirre et al. 1997). Typically, s corresponds to a 'boxcar' function indicating the stimulus is active/inactive while the HRF h may correspond to a Poisson or Gamma density (Glover 1999; Gössl et al. 2001; Smith and Fahrmeir 2007) in which case we have

$$x_{v,i} = \sum_{k=0}^{i-d_v} h(k, \lambda_v) s_{i-d_v-k} .$$

The parameters λ_v and d_v are usually estimated in a preprocessing step. A more sophisticated approach is to use an HRF consisting of a difference of two Gamma densities, one modeling the undershoot (Friston et al. 1998). Finally, $\varepsilon_{v,i}$ is the measurement error. Modeling the inherent spatial and temporal characteristics may be accomplished by making appropriate distributional assumptions for the $\varepsilon_{v,i}$ and through the choice of prior distributions for the parameters.

Detecting neuronal activation is now equivalent to detecting whether or not the coefficient β_v is nonzero, a variable selection problem (George and McCulloch 1993, 1997).

Others have taken similar approaches (Smith et al. 2003; Smith and Fahrmeir 2007) by modeling spatial association between neighboring voxels, but temporal correlation between the time series for each voxel is often ignored in the interests of computational efficiency. However, in Section 3 we show that this approach leads to lower quality inference. On the other hand, if one proceeds with a naive fully Bayesian approach which incorporates both spatial and temporal dependence it is easy to encounter posteriors that are computationally intractable even with the most sophisticated modern computational methods (see e.g. Lee 2010). Thus we are faced with a situation where computational issues drive some of the modeling decisions. In Section 2 we develop our model and pay careful attention to the prior specifications with the dual goals that we accurately reflect the nature of the experiment while mitigating the computational burden.

The posterior based on our prior specifications is typically of an extremely large dimension and is unavailable in closed form. We focus on the use of Markov chain Monte Carlo (MCMC) throughout to perform the required inferential tasks, but MCMC has its challenges. In particular, the high dimension of the posterior means that convergence is essentially impossible to verify using standard diagnostic methods. We derive a general MCMC algorithm which gives asymptotically correct answers and we investigate the effect of using several different priors on the performance of the MCMC algorithms and the resulting posterior inference.

We develop the Bayesian models and required MCMC algorithms in Section 2 and in Section 3 a simulation study is undertaken to validate the model and estimation procedure. Finally, we present the results of applying our methods to a particular data set in Section 4. Notably, we show how our model can allow for the task-related change in the BOLD signal to change dynamically over the scanning session. In this way, the model accounts for potential learning effects and other mechanisms of temporal drift in task-related signals. In the rest of this section we describe the fMRI experiment and resulting data that motivated our research and which is analyzed in Section 4.

1.1 Experimental fMRI Data

The experimental data are part of a longitudinal study of Alzheimer’s disease (AD) and its correlates. The study has been conducted in two waves of fMRI data collection with a third under way. All subjects provided informed consent, and the study was approved by the Johns Hopkins Medical Institutions Institutional Review Board. We investigate a color/word Stroop paradigm (Stroop 1935) implemented on a subset of the subjects in the second wave of data collection. To investigate normative values, we only consider right-handed controls in this study, as establishing normative activation is a necessary first step in producing biomarkers. All subjects are older, generally well-educated, and healthy. None of them have any clinically diagnosed neurologic disorders, including AD.

The Stroop test exploits the conflict between one well-learned or automatic behavior (e.g. reading) and a decision rule that requires this behavior be inhibited. Many previous behavioral studies have established the features of the Stroop task that produce cognitive

interference while neuroimaging studies (Bench et al. 1993; Carter et al. 1995; Fisher et al. 1990; Li et al. 2009; Polk et al. 2008; Taylor et al. 1997) have indicated that several brain regions are involved in the performance of the Stroop task, although these imaging studies do not all agree on which brain areas are most centrally involved in resolving Stroop inference.

Each subject in the current investigation performed the following Stroop task: subjects are shown words and subsequently asked to press a button corresponding to the color of the ink when the word is shown. There are three different components of the task:

- **Ink** only; the word is “XXXX” in colored ink; for example, when presented with **XXXX**, the subject will be expected to press the button for the color red.
- **Congruence**; the word is the color of the ink; for example, when presented with **BLUE**; the subject will be expected to press the button for the color blue.
- **Interference**; the word is a different color from the color of the ink; for example, when presented with **BLUE**, the subject will be expected to press the button for the color red.

This task considers an important cognitive mechanism; specifically, directed attention. Since most people are proficient at reading words, especially so in the highly educated sample under consideration, it takes inhibitory effort to ignore the word and concentrate on the color of the ink. Also, there is a well-documented age effect. That is, younger adults will typically experience a smaller interference effect than older adults. Additionally, interference effects may decrease with practice (Davidson et al. 2003). In this study all subjects are older so we will not model an age effect, but it may be of interest to describe any temporal drift in the response over the scanning session.

The Stroop exam was administered in the scanner in a block design (Friston et al. 2007) with a scanning time repetition of two seconds. The battery of Ink, Congruence and Interference were tasks repeated in sequence 3 times with observations taken at a total of 465 time points. We used standard fMRI preprocessing techniques, including slice timing (aligning axial slices via interpolation from the actual acquisition time), coregistration (using affine transformations to spatially normalize subjects images) and spatial smoothing. Data were then registered in standardized space. Template space is $79 \times 95 \times 68$ -dimensional with a voxel size of 2mm^3 .

Imaging data were subsequently masked, vectorized and stacked into a subject-specific matrix of time by voxels that represents our basic analytic structure. The mask was retained for back-transformation and visualization of results.

2 Variable Selection in a Spatio-Temporal Model

It is reasonable to expect that voxels are spatially dependent—voxels close together should behave similarly—and temporally dependent—the nature of the BOLD signal

suggests that voxels adjacent in time will have correlated responses and this effect will persist over longer time intervals than the scanning repetition time (Lund et al. 2006; Worsley et al. 2002; Woolrich et al. 2001). The model we develop below incorporates both characteristics.

Recall that for voxel $v = 1, \dots, N$ the BOLD image intensity at time $i = 1, \dots, T_v$ is $y_{v,i}$ and set $y_v = (y_{v,1}, \dots, y_{v,T_v})^T$. Let X_v be a known $T_v \times p$ matrix of full column rank and $\beta_v = (\beta_{v,1}, \dots, \beta_{v,p})^T$ be a $p \times 1$ vector of regression coefficients. We assume

$$y_v = X_v \beta_v + \varepsilon_v, \quad \varepsilon_v \sim N_{T_v}(0, \sigma_v^2 \Lambda_v). \quad (1)$$

Consider the structure of the design matrix X_v . We can account for long memory trends by introducing factors accounting for hardware related low-frequency drift, residual movement effects, and aliased physiological noise such as respiration and cardiac pulsation (Friston et al. 2007; Lund et al. 2006). Also, there are columns for each task corresponding to the convolution of the canonical HRF (Friston et al. 2007) with an impulse stimulus function (Rajapakse et al. 1998; Lindquist et al. 2009).

Our goal is detecting neuronal activation in a voxel which corresponds to identifying nonzero β_v . Let $\gamma_v = (\gamma_{v,1}, \dots, \gamma_{v,p})^T$ be binary random variables used to indicate whether the voxel is activated by a sequence of input stimuli. That is, the coefficient $\beta_{v,j}$ is equal to zero if $\gamma_{v,j} = 0$ and $\beta_{v,j}$ is nonzero if $\gamma_{v,j} = 1$. The zero of $\gamma_{v,j}$ implies no effect on voxel v is caused by the corresponding experimental task j . Therefore, the model in (1) can be written as

$$y_v = X_v(\gamma_v) \beta_v(\gamma_v) + \varepsilon_v, \quad \varepsilon_v \sim N_{T_v}(0, \sigma_v^2 \Lambda_v),$$

where $\beta_v(\gamma_v)$ is the vector of nonzero regression coefficients and $X_v(\gamma_v)$ is the corresponding matrix for a given indicator variable γ_v . That is, $X_v(\gamma_v)$ includes only the columns of X_v corresponding $\beta_{v,j}(\gamma_{v,j}) \neq 0$, $j = 1, \dots, p$.

We now turn our attention to specification of prior distributions. First consider the prior on $\beta_v(\gamma_v)$ given γ_v for a particular voxel, v . We will use Zellner's g -prior (Zellner 1996). This prior depends on a parameter typically denoted g which effectively controls model selection in that large values often lead to models with only a few large coefficients while small values tend to produce saturated models (Fernández et al. 2001; George 2000; Liang et al. 2008). We set this parameter equal to T_v yielding the unit information prior which leads to results similar to those if Bayesian information criterion (BIC) were used. Thus our prior is given by

$$\beta_v(\gamma_v) | y_v, \sigma_v^2, \Lambda_v, \gamma_v \sim N(\hat{\beta}_v(\gamma_v), T_v \sigma_v^2 [X_v^T(\gamma_v) \Lambda_v^{-1} X_v(\gamma_v)]^{-1}), \quad (2)$$

where

$$\hat{\beta}_v(\gamma_v) = [X_v^T(\gamma_v) \Lambda_v^{-1} X_v(\gamma_v)]^{-1} X_v^T(\gamma_v) \Lambda_v^{-1} y_v. \quad (3)$$

The prior is data-based because the mean depends on y_v . This prior often leads to simpler computation than alternative priors. For example, we also investigated the use

of multivariate t distributions, but these did not substantively change the results while making the required computation *much* more challenging (Lee 2010).

Next we assume the σ_v^2 are independent and

$$\pi(\sigma_v^2) \propto \frac{1}{\sigma_v^2}. \quad (4)$$

Note that Λ_v allows us to account for the temporal dependence between observations on a given voxel. We will see that the priors for Λ_v are critically important to both inferential efficacy and computational efficiency. Accordingly we will investigate the use of several priors. The first prior assumes no temporal dependence (i.e. Λ_v is an identity matrix), which is a common assumption made to achieve computational efficiency (Genovese 2000; Smith et al. 2003; Smith and Fahrmeir 2007).

While images are collected every 2 seconds the BOLD signal increases above baseline about 2 seconds after the onset of neuronal activity, peaking at about 5-8 seconds and falling below baseline for about 10 seconds. In addition to the persistence of neuronal activation it has been found that other cyclical neuronal events and artifacts of the measurement process can be responsible for temporal autocorrelation in fMRI settings (see e.g. Locascio et al. 1997). All of this suggests that an autoregressive (AR) or autoregressive moving average (ARMA) dependence might be sensible, but moving average processes, such as MA(1) or MA(2) processes, will be less desirable (see among many others Friston et al. 1995; Lindquist et al. 2009; Xia et al. 2009). In particular, we will focus on using AR(1) dependence so the (i, j) th element of Λ_v is $\Lambda_v(i, j) = \rho_v^{|i-j|}$. We will consider the use of two priors for $\rho = (\rho_1, \dots, \rho_N)$. The first assumes the components of ρ to be independently uniformly distributed between -1 and 1, that is,

$$\pi(\rho) = \prod_{v=1}^N \pi(\rho_v) \propto \prod_{v=1}^N I(-1 \leq \rho_v \leq 1).$$

The second prior we investigate will be based on an empirical Bayes (EB) approach where ρ is estimated with $\hat{\rho}$, the maximum likelihood estimator. This type of EB approach is often referred to as a *two-stage solution* or *prewhitening*.

We have investigated the use of other structures such as AR(2), ARMA(1,1) and MA(1) dependence, but using the EB approach with the AR(1) structure seems to be an effective compromise between inferential efficacy and computational efficiency. Indeed the robustness of our method is investigated in Section 3 while we compare the results in our real data application to that of using an empirical Bayes method (all parameters estimated with maximum likelihood) assuming AR(2), ARMA(1,1) and MA(1) dependence in Section 4.

All that remains is to specify a prior for the indicator variables γ_v . We will use a binary spatial Ising prior that allows us to incorporate anatomical prior information as well as spatial interaction between voxels. Let $\gamma_{(j)} = \{\gamma_{1,j}, \dots, \gamma_{N,j}\}$ be the vector of indicator variables for regression j over locations $\{1, 2, \dots, N\}$. We begin by addressing

how the spatial interaction is handled. Let $\omega_{v,k}$ be prespecified constants that allow us to weigh the interaction between neighboring locations on lattices v and k and let θ_j be the positive parameter to represent the strength of the interaction between any two voxels. If two voxels v and k are neighbors, then we write $v \sim k$ and the spatial interaction is described linearly

$$\theta_j \sum_{v \sim k} \omega_{v,k} I(\gamma_{v,j} = \gamma_{k,j}) .$$

The neighborhood structure is defined by the user. Commonly used neighborhood structures are based on the four, eight, or twelve nearest neighbors; see Figure 1. For

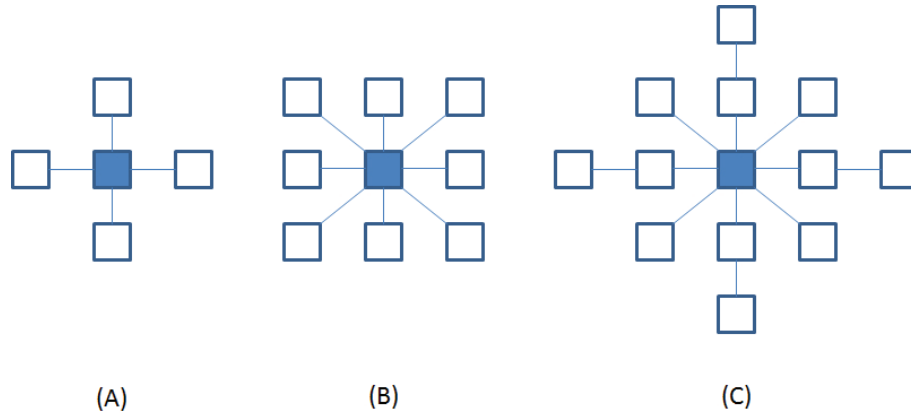


Figure 1: Common neighborhood structures in imaging analysis.

example, in the simulation study of Section 3 we employ a two-dimensional neighborhood of v that is defined to contain the directly adjacent vertical and horizontal voxels k . In our main application in Section 4 we employ a three-dimensional neighborhood that also includes the nine voxels immediately above, and nine voxels immediately below, voxel v . However, in any application the user should consider whether it may be more fruitful to consider cliques of higher orders instead of continuing the theme of pairwise interactions only; see [Tjelmeland and Besag \(1998\)](#) where several interesting experiments are conducted. We set the weights to be the reciprocal of the distance between voxel v and each of the neighboring voxels, but we also assess the robustness of this choice in Section 3.

Next we specify an “external field” which is meant to incorporate anatomical prior information in a linear combination of parameters

$$\sum_{v=1}^N \alpha_{v,j} \gamma_{v,j} .$$

The prior on γ is then taken to be $\pi(\gamma|\theta) = \prod_{j=1}^p \pi(\gamma_{(j)}|\theta_j)$, where

$$\pi(\gamma_{(j)}|\theta_j) \propto \exp \left\{ \sum_{v=1}^N \alpha_{v,j} \gamma_{v,j} + \theta_j \sum_{v \sim k} \omega_{v,k} I(\gamma_{v,j} = \gamma_{k,j}) \right\}, \quad (5)$$

where the $\alpha_{v,j}$ are chosen to reflect prior knowledge.

Smith and Fahrmeir (2007) consider the problem of incorporating external or anatomical information into the binary spatial Ising prior. We consider their approach in the current setting. To begin we will simplify the presentation by dropping the subscript j so that we are considering how to choose the parameters α_v in

$$\pi(\gamma|\theta) \propto \exp \left\{ \sum_{v=1}^N \alpha_v \gamma_v + \theta \sum_{v \sim k} \omega_{v,k} I(\gamma_v = \gamma_k) \right\}.$$

Now suppose that activation occurs only in some region G and introduce a indicator I_v to denote if the voxel v is in the area G , that is,

$$I_v = \begin{cases} 1, & v \in G; \\ 0, & \text{otherwise.} \end{cases}$$

Since activation only occurs in G it is reasonable to assume the marginal probability $p(\gamma_v = 1) = 0$ where $v \notin G$. On the other hand, we assume $p(\gamma_v = 1|I_v) = b_v$, $v \in G$ where b_v is specified by the user to reflect prior (including anatomical) knowledge. Further assume that the indicators are a priori independent across voxels. If voxel $v \in G$, we have

$$p(\gamma_v = 1) = p(\gamma_v = 1|I_v = 1)p(I_v = 1) = b_v \times p(I_v = 1) := e_v.$$

We match the marginal prior probabilities e_v to the external field of the Ising prior when there is no spatial correlation, so that $\theta = 0$. In this case the joint density is

$$\pi(\gamma|\theta = 0) = \exp \left\{ \sum_{v=1}^N \alpha_v \gamma_v \right\},$$

with marginals

$$\pi(\gamma_v = 1) = \frac{\exp\{\alpha_v\}}{1 + \exp\{\alpha_v\}} \stackrel{\text{set}}{=} e_v, \quad v \in G.$$

Therefore, an anatomically informed Ising prior is given by setting

$$\alpha_v = \log \frac{e_v}{1 - e_v}.$$

However, the drawback of using non-zero external field coefficients in the Ising prior is that θ is no longer simply a smoothing parameter. Therefore, we could employ a two-step procedure to address the relationship between θ and the marginal probability of activation with non-zero α_v :

Estimation Set $\alpha_1 = \dots = \alpha_N = 0$, estimate and obtain $\hat{\theta} = E(\theta|y)$.

Refitting Refit with an anatomically informed Ising prior, that is obtain $\alpha_1, \dots, \alpha_N$ as described above, but conditional on a fixed level of smoothing $\hat{\theta} = E(\theta|y)$.

This leaves only the distribution of the parameter θ to address. We assume a uniform prior on $\theta = (\theta_1, \dots, \theta_p)$, i.e., $\pi(\theta) \propto \prod_{j=1}^p I(0 < \theta_j < \theta_{\max})$, where θ_{\max} is a user-specified hyperparameter. In practice, $\theta_{\max} \leq 2$ often suffices; see Møller (2003).

Note that θ , ρ , and σ^2 are *a priori* independent, γ conditionally independent, and independence across voxels. Thus the posterior density is characterized by

$$\begin{aligned}
 q(\beta(\gamma), \gamma, \rho, \theta, \sigma^2|y) &\propto p(y|\beta(\gamma), \gamma, \sigma^2, \Lambda_v)\pi(\beta(\gamma)|y, \sigma^2, \Lambda, \gamma)\pi(\gamma|\theta)\pi(\rho)\pi(\sigma^2)\pi(\theta) \quad (6) \\
 &\propto \prod_{v=1}^N [p(y_v|\beta_v(\gamma_v), \gamma_v, \sigma_v^2, \Lambda_v)\pi(\beta_v(\gamma_v)|y_v, \gamma_v, \sigma_v^2, \Lambda_v)\pi(\sigma_v^2)] \\
 &\quad \times \pi(\gamma|\theta)\pi(\rho)\pi(\theta) .
 \end{aligned}$$

2.1 Posterior Inference

The posterior quantities of interest are the activation probability and its magnitude, that is, $q(\gamma_{v,j} = 1|y)$ and $E(\beta_v|y)$, respectively. These quantities are analytically intractable and must be approximated with Monte Carlo methods. We will describe a particular MCMC method in the subsequent section. A naive approach would be to construct an MCMC sampler having the full posterior $q(\beta(\gamma), \gamma, \rho, \theta, \sigma^2|y)$ as the invariant density. However, this would be computationally prohibitive. An alternative is to use Rao-Blackwellization. Note that

$$E(\beta_v|y) = \sum_{\gamma_v} E(\beta_v|\gamma_v, y)q(\gamma_v|y)$$

and if $\gamma_{-(v,j)}$ denotes the vector of binary regressors excluding $\gamma_{v,j}$, then

$$q(\gamma_{v,j} = 1|y) = \int q(\gamma_{v,j} = 1|\rho_v, \gamma_{-(v,j)}, y)q(\rho_v|y)q(\gamma_{-(v,j)}|y) d\rho_v d\gamma_{-(v,j)} .$$

Thus we only need an MCMC sampler whose invariant distribution is $q(\gamma, \rho|y)$. The MCMC algorithm will be described in the next section. For now, suppose

$$\{(\gamma^{[1]}, \rho^{[1]}), (\gamma^{[2]}, \rho^{[2]}), \dots, (\gamma^{[K]}, \rho^{[K]})\}$$

is a Monte Carlo sample generated with our MCMC algorithm. Then we can approximate the posterior quantities with

$$E(\beta_v|y) \approx \frac{1}{K} \sum_{k=1}^K \hat{\beta}_v(\gamma_v^{[k]}) \quad (7)$$

and

$$q(\gamma_{v,j} = 1|y) \approx \frac{1}{K} \sum_{k=1}^K q(\gamma_{v,j} = 1 | \gamma_{-(v,j)}^{[k]}, \rho_v^{[k]}, y) := \hat{q}(\gamma_{v,j} = 1|y). \quad (8)$$

How large should K be? There are two common approaches to choosing a value of K . The first is to fix a value of K before the simulation begins; that is, a fixed-time rule. The disadvantage of such a rule is that the user then has no control over the Monte Carlo error in the estimates. Another approach is to base the stopping rule on a fixed-width approach which continues the simulation until the Monte Carlo standard error (MCSE) is sufficiently small; see [Flegal and Gong \(2013\)](#), [Flegal and Jones \(2011\)](#), [Flegal et al. \(2008\)](#), and [Jones et al. \(2006\)](#). We will use the method of batch means to calculate asymptotically valid MCSEs.

We need a threshold in order to use \hat{q} to detect activation. Several authors have suggested using 0.8722, which we will use. That is, an individual voxel is categorized as active if $\hat{q} > 0.8722$, otherwise it is considered inactive. Following [Raftery \(1996\)](#), [Smith and Fahrmeir \(2007\)](#) give a clear description of the motivation for this value in the context of a Bayesian spatial model. In [Section 3](#) we compare this threshold value with some other possibilities and show that it is an effective choice.

2.2 Bayesian Inference via MCMC Sampling

We need to construct an MCMC sampler which has $q(\gamma, \rho|y)$ as the invariant density. Unfortunately, this density is not available in closed form since the integral

$$\int \pi(\gamma|\theta)\pi(\theta) d\theta$$

is analytically intractable. However, it will suffice to create an algorithm having $q(\gamma, \rho, \theta|y)$ as the invariant density. Let

$$S(\rho_v, \gamma_v) = (y_v - X_v(\gamma_v)\hat{\beta}_v(\gamma_v))^T \Lambda_v^{-1} (y_v - X_v(\gamma_v)\hat{\beta}_v(\gamma_v))$$

and $q_v = \sum_{j=1}^p \gamma_{v,j}$. In [Appendix 5](#) we show that

$$q(\gamma, \rho, \theta|y) \propto \pi(\gamma|\theta)\pi(\theta)\pi(\rho) \prod_{v=1}^N (1 + T_v)^{-q_v/2} |\Lambda_v|^{-1/2} S(\rho_v, \gamma_v)^{-T_v/2}.$$

As the target posterior may be truly high-dimensional it is natural to use a component-wise strategy ([Johnson et al. 2013](#)). In this case we need the three conditional densities

$q(\gamma|\rho, \theta, y)$, $q(\rho|\gamma, \theta, y)$ and $q(\theta|\gamma, \rho, y)$. These are characterized by

$$\begin{aligned}
 q(\gamma|\rho, \theta, y) &\propto \pi(\gamma|\theta) \prod_{v=1}^N (1 + T_v)^{-q_v/2} |\Lambda_v|^{-1/2} S(\rho_v, \gamma_v)^{-T_v/2} \\
 q(\rho|\gamma, \theta, y) &= q(\rho|\gamma, y) \propto \pi(\rho) \prod_{v=1}^N |\Lambda_v|^{-1/2} S(\rho_v, \gamma_v)^{-T_v/2} \\
 q(\theta|\gamma, \rho, y) &= q(\theta|\gamma, y) \propto \pi(\gamma|\theta)\pi(\theta) .
 \end{aligned}$$

Note that, given γ , θ and ρ are *a posteriori* independent. Let $\xi = (\theta, \rho)$. Then we can set up a two-variable component-wise sampler that updates γ followed by ξ ; that is, if we let (γ, ξ) be the current state and (γ', ξ') be the future state, one step of the MCMC sampler is the composition of two steps and looks like $(\gamma, \xi) \rightarrow (\gamma', \xi) \rightarrow (\gamma', \xi')$.

Step 1. Consider updating γ conditional on the values of θ and ρ . We will use a component-wise Metropolis-Hastings method. Schematically the transition $\gamma \rightarrow \gamma'$ consists of Np steps and will look like

$$\begin{aligned}
 &(\gamma_{1,1}, \gamma_{2,1}, \dots, \gamma_{N,1}, \dots, \gamma_{1,p}, \gamma_{2,p}, \dots, \gamma_{N,p}) \\
 &\rightarrow (\gamma'_{1,1}, \gamma_{2,1}, \dots, \gamma_{N,1}, \dots, \gamma_{1,p}, \gamma_{2,p}, \dots, \gamma_{N,p}) \\
 &\rightarrow (\gamma'_{1,1}, \gamma'_{2,1}, \dots, \gamma_{N,1}, \dots, \gamma_{1,p}, \gamma_{2,p}, \dots, \gamma_{N,p}) \\
 &\quad \vdots \\
 &\rightarrow (\gamma'_{1,1}, \gamma'_{2,1}, \dots, \gamma'_{N,1}, \dots, \gamma'_{1,p}, \gamma'_{2,p}, \dots, \gamma'_{N,p}) .
 \end{aligned}$$

Thus we need the density $q(\gamma_{v,j}|\gamma_{-(v,j)}, \theta, \rho, y)$. Notice that

$$\begin{aligned}
 q(\gamma_{v,j}|\gamma_{-(v,j)}, \theta, \rho, y) &\propto (1 + T_v)^{-\gamma_{v,j}/2} S(\rho_v, \gamma_v)^{-T_v/2} \\
 &\quad \times \exp \left\{ \alpha_{v,j} \gamma_{v,j} + \theta_j \sum_{k \in \delta_v} \omega_{v,k} I(\gamma_{k,j} = \gamma_{v,j}) \right\} .
 \end{aligned}$$

Now let $p_{\gamma_{v,j}}(\cdot|\gamma_{-(v,j)}, \theta, \rho)$ be a user-specified proposal distribution. Then one of the Np steps occurs as follows. Let the current state of the Markov chain be

$$\gamma = (\gamma'_{1,1}, \dots, \gamma'_{v,j-1}, \gamma_{v,j}, \gamma_{v,j+1}, \dots, \gamma_{N,p}) .$$

Then draw proposal $\gamma_{v,j}^* \sim p_{\gamma_{v,j}}(\cdot|\gamma_{-(v,j)}, \theta, \rho)$. Set $\gamma'_{v,j} = \gamma_{v,j}^*$ with probability the minimum of 1 and the Hastings ratio, otherwise set $\gamma'_{v,j} = \gamma_{v,j}$. The Hastings ratio is

$$\begin{aligned}
 &\frac{(1 + T_v)^{-\gamma_{v,j}^*/2} S(\rho_v, \gamma_{-(v,j)}, \gamma_{v,j}^*)^{-T_v/2}}{(1 + T_v)^{-\gamma_{v,j}/2} S(\rho_v, \gamma_v)^{-T_v/2}} \\
 &\quad \times \frac{\exp \{ \alpha_{v,j} \gamma_{v,j}^* + \theta_j \sum_{k \in \delta_v} \omega_{v,k} I(\gamma_{k,j} = \gamma_{v,j}^*) \} p_{\gamma_{v,j}}(\gamma_{v,j}|\gamma_{-(v,j)}, \theta, \rho)}{\exp \{ \alpha_{v,j} \gamma_{v,j} + \theta_j \sum_{k \in \delta_v} \omega_{v,k} I(\gamma_{k,j} = \gamma_{v,j}) \} p_{\gamma_{v,j}}(\gamma_{v,j}^*|\gamma_{-(v,j)}, \theta, \rho)} .
 \end{aligned}$$

Notice that no matter which proposal distribution $p_{\gamma_{v,j}}$ we use, if $\gamma_{v,j}^* = \gamma_{v,j}$, then the Hastings ratio is 1 and we automatically set $\gamma'_{v,j} = \gamma_{v,j}^*$.

One possible choice for the proposal distribution is

$$p_{\gamma_{v,j}}(\gamma_{v,j}|\gamma_{-(v,j)}, \theta, y) = \frac{1}{Z(\theta)} \exp \left\{ \alpha_{v,j} \gamma_{v,j} + \theta_j \sum_{k \in \delta_v} \omega_{v,k} I(\gamma_{k,j} = \gamma_{v,j}) \right\}$$

from which it can be shown that

$$p_{\gamma_{v,j}}(\gamma_{v,j} = 1|\gamma_{-(v,j)}, \theta, y) = \left[1 + \exp \left\{ -\alpha_{v,j} + \theta_j \sum_{k \in \delta_v} \omega_{k,v} (1 - 2\gamma_{k,j}) \right\} \right]^{-1}.$$

This leads to a simplification in the Hastings ratio

$$\frac{(1 + T_v)^{-\gamma_{v,j}^*/2} S(\rho_v, \gamma_{-(v,j)}, \gamma_{v,j}^*)^{-T_v/2}}{(1 + T_v)^{-\gamma_{v,j}/2} S(\rho_v, \gamma_v)^{-T_v/2}}.$$

Step 2. Consider updating ρ conditional on γ . In this step we again use a component-wise MCMC algorithm. Schematically the transition $\rho \rightarrow \rho'$ consists of N steps and will look like

$$\begin{aligned} (\rho_1, \rho_2, \dots, \rho_{N-1}, \rho_N) &\rightarrow (\rho'_1, \rho_2, \dots, \rho_{N-1}, \rho_N) \\ &\rightarrow (\rho'_1, \rho'_2, \dots, \rho_{N-1}, \rho_N) \\ &\vdots \\ &\rightarrow (\rho'_1, \rho'_2, \dots, \rho'_{N-1}, \rho_N) \\ &\rightarrow (\rho'_1, \rho'_2, \dots, \rho'_{N-1}, \rho'_N). \end{aligned}$$

Thus we need the density $q(\rho_v|\rho_{-v}, \gamma, y)$. Notice that

$$q(\rho_v|\rho_{-v}, \gamma, y) = q(\rho_v|\gamma, y) \propto \pi(\rho_v) |\Lambda_v|^{-1/2} S(\rho_v, \gamma_v)^{-T_v/2}.$$

Let the current state of the Markov chain be ρ_v . Then generate a proposal ρ_v^* from the density $p_{\rho_v}(\cdot|\gamma, y)$ and set $\rho'_v = \rho_v^*$ with probability the minimum of 1 and the Hastings ratio which is given by

$$\frac{\pi(\rho_v^*) |\Lambda_v^*|^{-1/2} S(\rho_v^*, \gamma_v)^{-T_v/2} p_{\rho_v}(\rho_v|\gamma, y)}{\pi(\rho_v) |\Lambda_v|^{-1/2} S(\rho_v, \gamma_v)^{-T_v/2} p_{\rho_v}(\rho_v^*|\gamma, y)}.$$

Otherwise, set $\rho'_v = \rho_v$. One possible choice for the proposal density is a uniform distribution, $\text{Uniform}(-1, 1)$.

Notice that when we use the EB approach for ρ we avoid this step entirely.

Step 3. Consider updating θ conditional on γ . Again we use a component-wise MCMC method. Schematically the transition $\theta \rightarrow \theta'$ consists of p steps and looks like

$$\begin{aligned} (\theta_1, \theta_2, \dots, \theta_{p-1}, \theta_p) &\rightarrow (\theta'_1, \theta_2, \dots, \theta_{p-1}, \theta_p) \\ &\rightarrow (\theta'_1, \theta'_2, \dots, \theta_{p-1}, \theta_p) \\ &\vdots \\ &\rightarrow (\theta'_1, \theta'_2, \dots, \theta'_{p-1}, \theta_p) \\ &\rightarrow (\theta'_1, \theta'_2, \dots, \theta'_{p-1}, \theta'_p) . \end{aligned}$$

Thus we need the density $q(\theta_j|\theta_{-j}, \gamma, y)$. Notice that

$$\begin{aligned} q(\theta_j|\theta_{-j}, \gamma, y) &= q(\theta_j|\gamma, y) \\ &\propto Z_j^{-1}(\theta_j, \alpha_j) \exp \left\{ \theta_j \sum_{v \sim k} \omega_{v,k} I(\gamma_{v,j} = \gamma_{k,j}) \right\} I(0 < \theta_j < \theta_{\max}) . \end{aligned}$$

where

$$Z_j(\theta_j, \alpha_j) = \left[\sum_{\gamma_{(j)}} \exp \left\{ \sum_{v=1}^N \alpha_{v,j} \gamma_{v,j} + \theta_j \sum_{v \sim k} \omega_{v,k} I(\gamma_{v,j} = \gamma_{k,j}) \right\} \right] .$$

Let the current state of the Markov chain be θ_j . Then generate a proposal θ_j^* from a proposal density $p_{\theta_j}(\cdot|\gamma, y)$. Then set $\theta'_j = \theta_j^*$ with probability the minimum of 1 and the Hastings ratio

$$\frac{Z_j(\theta_j, \alpha_j) \exp \{ \theta_j^* \sum_{v \sim k} \omega_{v,k} I(\gamma_{v,j} = \gamma_{k,j}) \} I(0 < \theta_j^* < \theta_{\max}) p_{\theta_j}(\theta_j|\gamma, y)}{Z_j(\theta_j^*, \alpha_j) \exp \{ \theta_j \sum_{v \sim k} \omega_{v,k} I(\gamma_{v,j} = \gamma_{k,j}) \} I(0 < \theta_j < \theta_{\max}) p_{\theta_j}(\theta_j^*|\gamma, y)} .$$

The ratio

$$\frac{Z_j(\theta_j, \alpha_j)}{Z_j(\theta_j^*, \alpha_j)}$$

is analytically intractable but can be estimated with path sampling (Gelman 1998) or the Wang-Landau algorithms (Wang and Landau 2001; Zhang and Ma 2007), among others.

One choice for a proposal distribution is $N(\theta_j, \tilde{\sigma}^2)$ where θ_j is the current state and $\tilde{\sigma}$ will be tuned so that the acceptance rate is roughly 40%.

3 Simulation Study

In this section we report the results of a simulation study undertaken to validate the model and estimation procedure described above. In part this is done to investigate what differences arise when different priors are used for ρ . Specifically, we consider the 3 cases where (i) $\rho_v \sim \text{Uniform}(-1, 1)$, independently; (ii) an empirical Bayes approach

is used to estimate ρ with $\hat{\rho}$, which is calculated by maximum likelihood; and (iii) taking Λ_v to be the identity matrix for all v . In the second part of this section we continue to use the EB approach and investigate the robustness of our choice for the weights $\omega_{v,k}$ in our spatial prior and our choice of .8722 for the cutoff for the posterior activation probabilities. The final part of this section is concerned with investigating the robustness of either (i) using an empirical Bayes approach to estimate ρ with $\hat{\rho}$ or (ii) taking Λ_v to be the identity matrix for all v when the underlying data is generated with various temporal correlation structures.

We generate 10 data sets from the model based on 30×30 activated-inactivated images. We do *a posteriori* inference on these data sets using the full posterior defined at (6). We then compare the various methods based on their ability to estimate the spatial interaction parameter θ and their ability to correctly classify voxels as activated or inactivated.

We now describe how we generate the data. Suppose $\sigma_v = \sigma^2$ for each $v = 1, \dots, N$ and set $(\theta, \sigma^2) = (.7, 3)$. Given θ , a γ is exactly generated from

$$p(\gamma|\theta) = \frac{1}{Z(\theta)} \exp \left\{ \theta \sum_{i \sim j} \omega_{i,j} I(\gamma_i = \gamma_j) \right\}.$$

Simulating from $p(\gamma|\theta)$ is not easy but can be done using a perfect sampling technique for Ising models (Propp and Wilson 1996). This γ is a 30×30 activated-inactivated square image. Given γ , we simulate a time-series y_v in each voxel v of length 100 from the model

$$y_v = X_v(\gamma_v)\beta_v(\gamma_v) + \varepsilon_v, \quad \varepsilon_v \sim N_{100}(0, \sigma_v^2 \Lambda_v).$$

We assume a ‘boxcar’ type stimulus function and after convolving with the canonical HRF the design matrix is given in Figure 2.

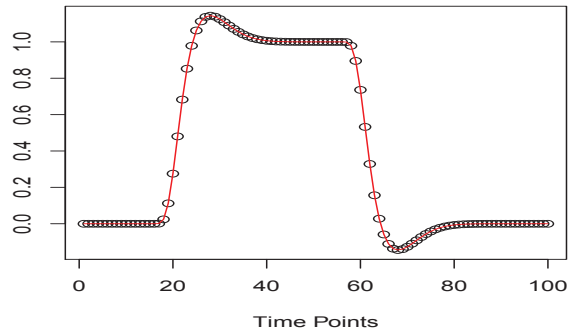


Figure 2: The design matrix used in the simulation study.

The autoregression coefficient, ρ_v , is generated from $\text{Uniform}(-1, 1)$ for each voxel. Let $\beta_v = (\beta_{v,0}, \beta_{v,1})^T$ where $\beta_{v,0}$ represents the baseline level and $\beta_{v,1}$ describes the amplitude of activation in response to a stimulus at each voxel v . We use $\gamma_{v,j}$ to indicate if $\beta_{v,j}$ is equal to 0 or not, that is, $\beta_{v,j} \neq 0$ if $\gamma_{v,j} = 1$; otherwise $\beta_{v,j} = 0$. In this simulation, we always assume $\gamma_{v,0} = 1$ since $\beta_{v,0}$ models the baseline level in a human brain. On the other hand, $\gamma_{v,1}$ can be either 0 or 1. When $\gamma_{v,1} = 1$, we set $\beta_v = (300, 5)^T$; otherwise $\beta_v = \beta_{v,0} = 300$. The reason we set $\beta_{v,1} = 5$ is that the BOLD contrast is typically fairly small, with activation inducing a signal increase ranging from 1% to 5%.

For each simulated data set, the spatial Bayesian variable selection approach is applied to detect the activation and to estimate the spatial coefficient θ via its posterior mean. Recall the prior for β is given in (2). Now consider the binary spatial Ising prior (5). We used a two-dimensional neighborhood which contains the directly adjacent voxel and the horizontal voxels. The weights $\omega_{v,k}$ were taken to be the reciprocal of the distance between voxels v and k . Finally, we set $\theta_{\max} = 2$ and since there is no anatomical information in this problem we set $\alpha = 0$. To evaluate the performance of this method, we consider the accuracy of estimating θ with its posterior mean and the accuracy and false positive rate of identifying activation-inactivation. Note that we classified a voxel as active if $\hat{q} > 0.8722$. Accuracy is defined as the percentage of voxels correctly classified. The false positive rate is the percentage of active voxels falsely identified.

The average estimates of θ and corresponding Monte Carlo standard errors (MCSEs) over 10 simulated data are given in Table 1. Recall that the true value for θ is 0.7. The estimation results are based on 1×10^4 draws from the posterior using our MCMC algorithm, resulting in all MCSEs being less than 0.005. The results suggest that using a prior which does not include temporal correlation (i.e. $\Lambda_v = I_{100}$) will lead to overestimates of the spatial correlation but there is little difference between either of the other two priors.

Prior for ρ	Estimate $\hat{\theta}$	MCSE
$\text{Uniform}(-1, 1)$	0.73	0.0017
EB	0.74	0.0015
$\Lambda_v = I_{100}$	0.78	0.0015

Table 1: The average Monte Carlo estimates of θ and corresponding Monte Carlo standard errors (MCSE) based on 1×10^4 MCMC iterations for each of the 10 simulated data sets.

Table 2 reports the average (over times and data sets) accuracy and false positive rate for each of the 3 priors. Again we find that ignoring the temporal correlation will lead to inferior inference. Specifically, when $\Lambda_v = I_{100}$ we observed a higher false positive rate. However, the other two priors produce comparable results. It is worth emphasizing that the computation time required for the EB approach is over 300 times less than that required for the $\text{Uniform}(-1, 1)$ prior; note that with the EB method Step

2 of the MCMC algorithm is superfluous so inversion of Λ_v for each voxel is avoided.

Prior for ρ	$\Lambda_v = I_{100}$	Uniform(-1, 1)	EB
Accuracy (%)	91.38	97.38	97.16
False Positive Rate (%)	13.59	0.045	0.04

Table 2: The accuracy based on 1×10^4 MCMC iterations for each of the 10 simulated data sets.

We next use the EB method for estimating ρ and assess the robustness of the procedure to our choice of weights $\omega_{v,k}$ and activation cutoff $\hat{q} > 0.8722$.

Consider our choice for the weights $\omega_{v,k}$, which is the reciprocal of the Euclidian distance between voxels. We tried half and double these values of $\omega_{v,k}$ in our simulation study. Both show quite similar results to the weights we chose previously. The choice of weights does not appear to significantly impact the quality of the inference in this example. The results are reported in Table 3.

Weight	1/2	1	2
Accuracy (%)	97.11	97.28	97.25
False Positive (%)	1.20	1.36	1.34

Table 3: The accuracy and false positive rate on identifying activation corresponding to different weights applied where original means the weights are equal to the reciprocal of the distance between voxels, half for half original weights, double for double original weights.

To investigate the effect of the choice of the threshold on the result, a sensitivity study in terms of accuracy of identification of activation is given. The voxel is activated if the corresponding posterior probability $\hat{q}(r = 1|y)$ is greater than a specified value. Letting $p = q(r = 1|y)$, we have

$$-2 \log \left(\frac{1-p}{p} \right) \overset{appr.}{\sim} \chi^2(1).$$

We tried a set of p -values of .01, .05, and .1 with corresponding critical values of 6.635, 3.841, and 2.705, respectively. Given the critical values, the posterior probabilities $q(r = 1|y)$ are equal to .9650, .8722, .7946, respectively. Then we applied the critical values to detect the activation. Table 4 shows the results. Based on these results, it seems reasonable to take the threshold as 0.8722.

Critical value	.7946	.8722	.9650
Accuracy (%)	97.44	97.28	95.93
False Positive (%)	2.30	1.36	0.50

Table 4: The accuracy of detection of activation using different critical values.

To this point all of our simulated data has followed an autoregressive temporal correlation. We now turn our attention to assessing the robustness of our procedure when this assumption does not hold. Specifically, we simulated 100 images under each of 5 temporal correlation structures—AR(1), AR(2), MA(1), MA(2) and ARMA(1,1). We then fit two models to each data set. One of the models was our EB method assuming an AR(1) temporal correlation and one was a model which assumed no temporal correlation. The results are presented in Tables 5 and 6. Yet again we see that ignoring the temporal correlation results in inferior inference. It is also clear from these results that the use of an AR(1) structure is quite reasonable in all of these settings.

Models	AR(1)	AR(2)	MA(1)	MA(2)	ARMA(1, 1)
Acc (%)	97.38 (0.97)	96.40 (0.97)	95.98 (0.67)	97.88 (1.75)	96.01 (0.65)
FP (%)	0.68 (0.041)	2.23 (0.077)	0.97 (0.041)	0.98 (0.067)	0.97 (0.043)

Table 5: The EB AR(1) model is implemented on 100 images simulated with five different temporal correlation structures. The accuracy (Acc) and false positive (FP) rates are reported. The figures inside of parentheses are the corresponding MCSE.

Models	AR(1)	AR(2)	MA(1)	MA(2)	ARMA(1, 1)
Acc (%)	95.11 (1.26)	94.43 (1.47)	98.56 (0.07)	96.88 (0.08)	93.67 (1.65)
FP (%)	8.74 (0.41)	10.22 (0.87)	0.10 (0.004)	6.00 (0.64)	9.79 (1.43)

Table 6: The model with $\Sigma = I$ is implemented on 100 images simulated with five different temporal correlation structures. The accuracy (Acc) and false positive (FP) rates are reported. The figures inside of parentheses are the corresponding MCSE.

4 Activation in Experimental fMRI Data

In this section we use the methodology, i.e. the model, estimation procedure and the MCMC sampling method, described earlier to analyze the Stroop data which was described in Section 1.1. Based on the results of Section 3 we will limit attention to using EB methods for ρ ; recall that we found little difference in the quality of inference between the EB approach and the Uniform prior while the computing time for the EB method was over 300 times less. The weights in the binary spatial Ising prior will be given by the reciprocal of the Euclidean distance between neighboring voxels and set $\theta_{\max} = 1$. We used a cutoff of .8772 for detecting activation.

We consider two different models in this section. The first (see Section 4.2) does not allow for changes in the activation patterns over time while the second (see Section 4.3) does. Which model is used should be determined by the inferential goals. If the interest is mainly in which areas are activated by a task, the time-invariant model should be used. But if we want investigate the activation changes over time, the time-varying model is appropriate.

4.1 Design Matrix in the Regression Model

In general, at voxel v , the design matrix X_v consists of the effects of no interest, transformed stimuli, and the baseline trend. The transformed stimulus is the convolution of the stimulus function with the assumed HRF, as discussed earlier. In this fMRI experiment, there are 3 types of tasks (“Ink Only”, “Congruence”, and “Interference”) given 3 alternating times. Therefore, this part of the design matrix implemented in this study was obtained by convolving the stimulus function with the canonical HRF. The visualization of the design matrix is given in Figure 3. The red and black lines in Figure 3 model the initial effect which is of no interest and the baseline trend during the experiment, respectively. The green, blue, and pink lines model the corresponding effects, “Ink Only”, “Congruence”, and “Interference” during the test.

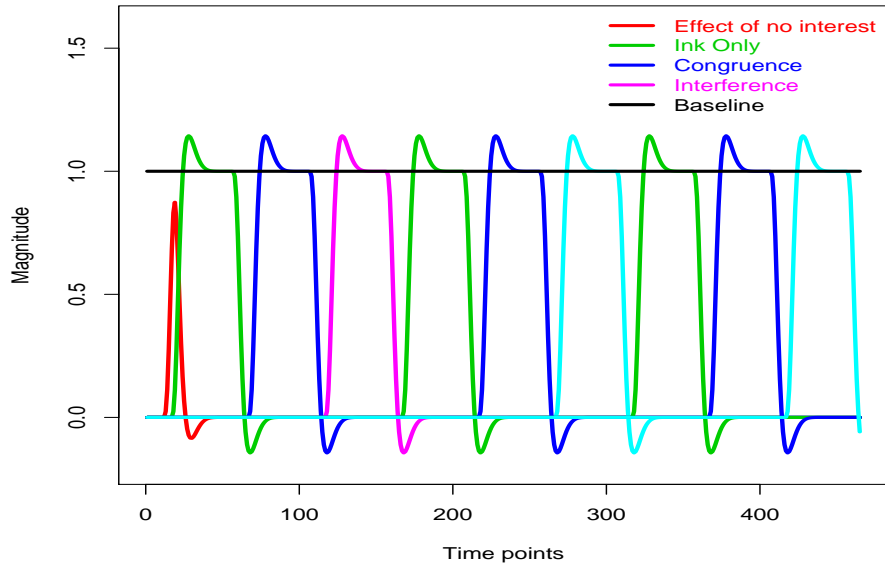


Figure 3: The design matrix used for the experimental fMRI data.

4.2 Time-Invarying Activation Patterns

We assume the basic linear model

$$y_v = a_0 z_0 + a_1 z_1 + \beta_1 x_1 + \beta_2 x_2 + \beta_3 x_3 + \varepsilon_v, \quad (9)$$

where y_v represents a time-series in a particular voxel v , each x_i is a transformed input function, z_i is a vector used to remove low-frequency, stimulus independent effects, the

β_i are parameters of interest corresponding to different tasks, “Ink Only”, “Congruence”, and “Interference”, respectively. The a_i are nonzero nuisance parameters to model the baseline brain signal. The rest of the hierarchical model is specified as described in Section 2 and at the beginning of this section. A sequence of binary variables $\gamma_v = \{1, 1, \gamma_{3,v}, \gamma_{4,v}, \gamma_{5,v}\}$ is used to indicate if the corresponding parameter is zero or not; recall that we assume both of the a_i are nonzero.

The posterior of interest $q(\gamma, \theta|y)$ is intractable so we will use the MCMC algorithm developed in Section 2.2 to obtain 1×10^5 observed values of the Markov chain. We use the method of batch means (Jones et al. 2006) to calculate MCSEs for the estimated quantities. We also used trace plots and histograms to visually assess convergence of the simulation.

The estimates of the components of the spatial correlation parameter are given in Table 7. Note that the reported MCSEs are small and hence we have precise estimates. Also, the spatial correlations appear quite large.

θ_2	θ_3	θ_4
0.7476 (0.00006)	0.7520 (0.00006)	0.6181 (0.00007)

Table 7: Estimate of the components of θ based on 1×10^5 MCMC simulations with MCSE given in the parentheses.

In Figure 4 we present some results predicting activation from the coronal, sagittal, axial, and whole brain views. Figure 4(A), 4(B), and 4(C) show predicted activations while performing the “Ink Only”, “Congruence”, and “Interference” tasks, respectively. The parietal and occipital lobes are activated during the Stroop task since the parietal lobe accounts for cognition, information processing, and visual perception and the occipital lobe is the visual processing center which is responsible for control of vision and color recognition. Additionally, the activation regions in the right brain are larger than those in the left brain partly because the left and right hemispheres of the brain process information in different ways and we tend to process information using our dominant side; recall that all subjects were right-handed.

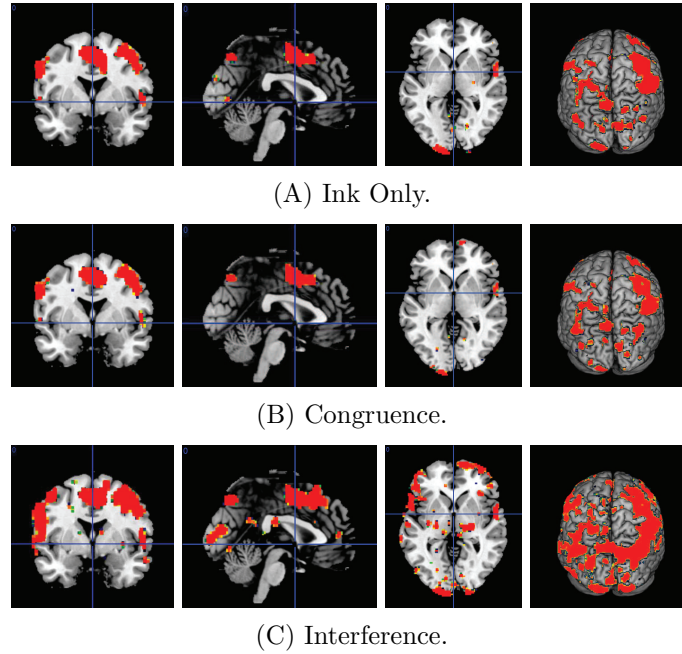


Figure 4: Predicted activation maps for each task using AR(1) temporal dependence.

4.3 Time-Varying Activation Patterns

In the fMRI experiment described in Section 1, the three different Stroop tasks are repeated three times. The model at (9) fails to serve the goal of studying a possible activation change over time. Here we generalize the model in order to study possible changes to the activation pattern over time. Suppose,

$$\begin{aligned}
 Y_v = & a_0 z_0 + a_1 z_1 + \beta_{1,1} x_{1,1} + \beta_{1,2} x_{1,2} + \beta_{1,3} x_{1,3} + \beta_{2,1} x_{2,1} + \beta_{2,2} x_{2,2} + \beta_{2,3} x_{2,3} \\
 & + \beta_{3,1} x_{3,1} + \beta_{3,2} x_{3,2} + \beta_{3,3} x_{3,3} + \varepsilon_v,
 \end{aligned} \tag{10}$$

where $x_{i,j}$ is the transformed input function of task j in the i th trial, z_i is a vector used to remove low-frequency, stimulus independent effects, $\beta_{i,j}$ is the parameter of interest corresponding to the j th task in the i th trial, the a_i are nonzero nuisance parameters to model the baseline of a brain signal and ε_v has a normal distribution, $N(0, \sigma_v^2 \Lambda_v)$. We continue to use the EB method based on the MLE $\hat{\rho}$ for the elements of Λ_v . A sequence of binary variables is used to indicate if the corresponding parameter is zero or not. In our case, we assume a_i nonzero. Therefore, the variable for voxel v is

$$\gamma_v = \{1, 1, \gamma_{3,v}, \gamma_{4,v}, \gamma_{5,v}, \gamma_{6,v}, \gamma_{7,v}, \gamma_{8,v}, \gamma_{9,v}, \gamma_{10,v}, \gamma_{11,v}\}.$$

The rest of the model specification is as described in Section 2.

The posterior of interest $q(\gamma, \theta|y)$ is intractable so we will use the MCMC algorithm developed in Section 2.2 to obtain 1×10^5 observed values of the Markov chain. We use

the method of batch means (Jones et al. 2006) to calculate MCSEs for the estimated quantities. We also used trace plots and histograms to visually assess convergence of the simulation.

The activation maps are given in Figures 5, 6, and 7. All these figures show that the partial lobe is activated during these tasks in different phases but the occipital lobe is only activated in the third trial and the frontal lobe is slightly activated in the first trial of congruence and interference tasks and in the second trial of ink only task. The temporal lobe is only activated in the third phase, not in the first and second phases. Notice that the size of activation areas when performing the “Interference” task is bigger than that when performing the other two.

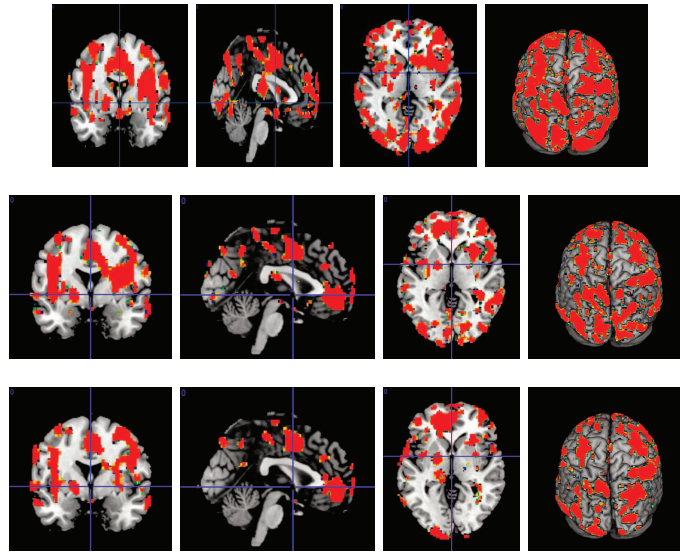


Figure 5: Activation maps for the time-varying model in the first trial. The top row is activation maps when performing the “Ink Only” task, the middle one for the “Congruence” task, and the bottom one for the “Interference” task.

4.4 Model Assessment

To keep things manageable we will limit discussion to the model in Section 4.2. Similar results were found for the model in Section 4.3. We performed several voxel-level exploratory analyses to assess model fit. For example, we plotted the raw data versus time with a trend line, residuals as a function of time, quantile-quantile plots to assess our distributional assumption of normality and autocorrelation function (ACF) and partial ACF plots to assess the temporal correlation. We present the results for several randomly selected voxels in Figures 8 and 9. Consider Figure 8. The first row of each plot is the raw data with a fit line. The second row is the residual multiplied by

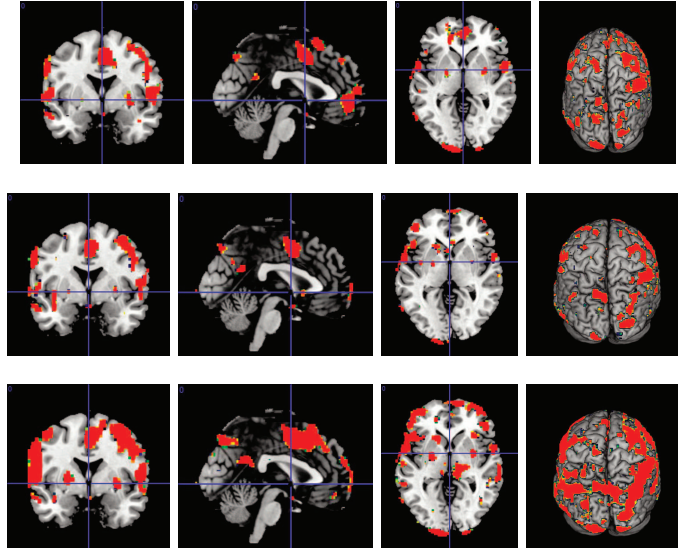


Figure 6: Activation maps for the time-varying model in the second trial. The top row is activation maps when performing the “Ink Only” task, the middle one for “Congruence” task, and the bottom one for the “Interference” task.

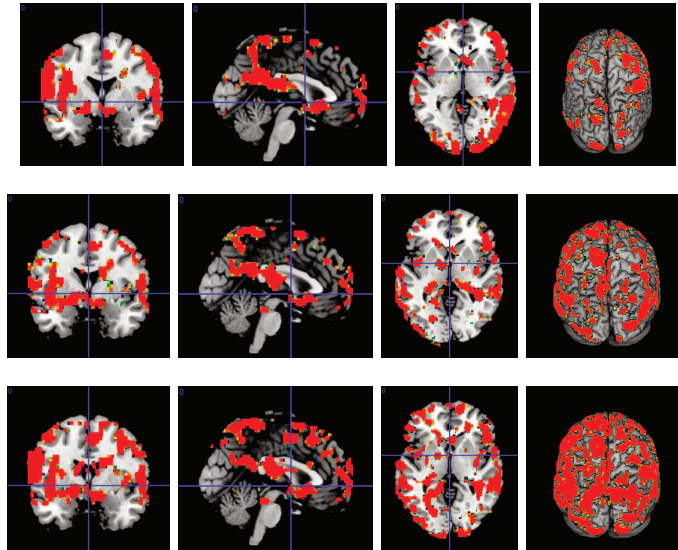


Figure 7: Activation maps for the time-varying model in the third trial. The top row is activation maps when performing the “Ink Only” task, the middle one for the “Congruence” task, and the bottom one for the “Interference” task.

the inverse squared root of AR(1) covariance and the quantile-quantile plots for the corresponding residuals with a Shapiro–Wilk test given. Even when the Shapiro–Wilk test rejects normality, we find by checking the quantile-quantile plots that most of the points lie around the straight line. Now consider Figure 9 which contains the ACF and PACF plots for the same voxels as in Figure 8. Mostly this shows that an AR(1) structure is reasonable although a couple suggest that a higher order autoregressive structure could be appropriate.

We also performed voxel-wise chi-squared goodness-of-fit tests by comparing the reduced model to the full model at the .1 level, very few (.01%) of the null hypotheses (reduced model) were rejected. In addition, only a small percentage (0.05%) of the voxels had BIC values that were smaller for the reduced model than for the full model. Finally, we examined the nature of the activation patterns with the 3 possible cutoff probabilities (i.e. .9650, .8722 and .7946) introduced in Section 3 and found little practical difference in the patterns. In sum, these analyses suggest that our model fits the data reasonably well.

Recall that in Section 4.2 we used EB methods for all of the ρ_v and assumed *a priori* that the ρ_v are independent across voxels. This was done mainly because the simulation study results from Section 3 suggested that the quality of inference was similar when we assumed $\rho_v \sim \text{Uniform}(-1, 1)$, independently. Moreover, when we tried to use the Uniform priors on the experimental fMRI data the computation was prohibitively expensive. The crux of the computational issue can be seen by examining the Hastings ratio for the MCMC step updating ρ_v

$$\frac{\pi(\rho_v^*)|\Lambda_v^*|^{-1/2}S(\rho_v^*, \gamma_v)^{-T_v/2} p_{\rho_v}(\rho_v|\gamma, y)}{\pi(\rho_v)|\Lambda_v|^{-1/2}S(\rho_v, \gamma_v)^{-T_v/2} p_{\rho_v}(\rho_v^*|\gamma, y)}$$

where $S(\rho_v, \gamma_v) = (y_v - X_v(\gamma_v)\hat{\beta}_v(\gamma_v))^T \Lambda_v^{-1}(y_v - X_v(\gamma_v)\hat{\beta}_v(\gamma_v))$. Although computing the determinant of Λ_v is easy and fast, calculating $S(\rho_v, \gamma_v)$ is time consuming partly because Λ_v must be inverted. In the current fMRI data example Λ_v is 465×465 and it must be inverted for each voxel.

However, the assumption of independence of the ρ_v may not be optimal. Figure 10 shows the MLE for ρ_v in each voxel. There does seem to be some evidence that nearby voxels tend to have similar values and hence the map may be exhibiting spatial correlation. It would be a potentially interesting research project to try to account for this through a prior specification on ρ while maintaining computational feasibility.

Finally, we compare the activation maps produced from our model when different temporal structures, AR(2), ARMA(1,1), and MA(1), are assumed. In each case we used maximum likelihood estimates of the parameters and implemented an empirical Bayes approach. The computational effort for each of these was similar to that of the EB AR(1) model. The results are presented in figures in the Supplemental Material. The activation maps for the AR(1) and AR(2) models are comparable, but the ARMA(1,1) and MA(1) activation maps show larger activated regions. Given the results of the ACF and PACF plots above as well as the results of the simulation study in Section 3 we suspect that the ARMA(1,1) and MA(1) fits are yielding a substantial number of false

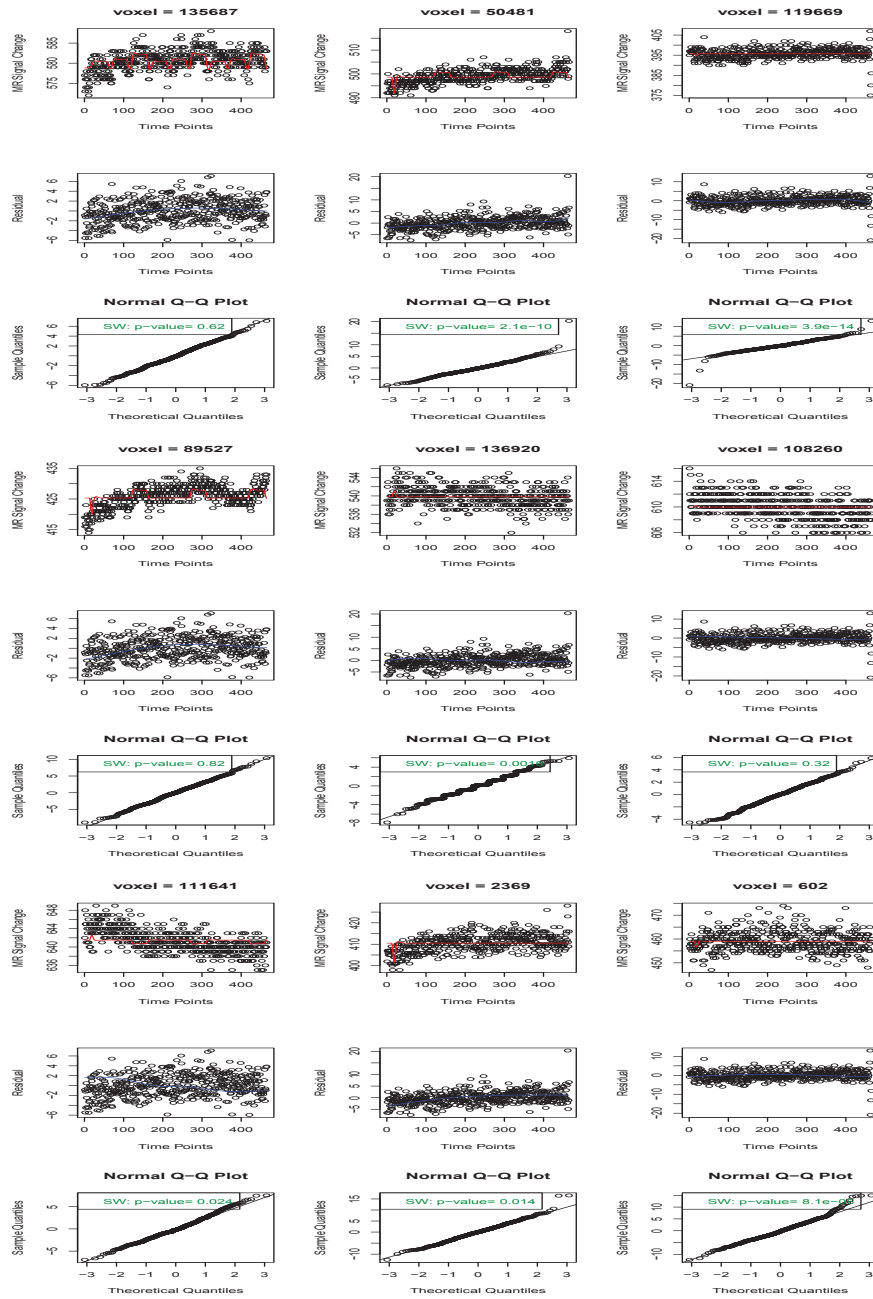


Figure 8: Residual check. The 1st, 4th, 7th rows represent the raw data with a fit line, 2nd, 5th, 8th are the corresponding residuals with a spline, and 3rd, 6th, 9th rows are the corresponding QQ plots.

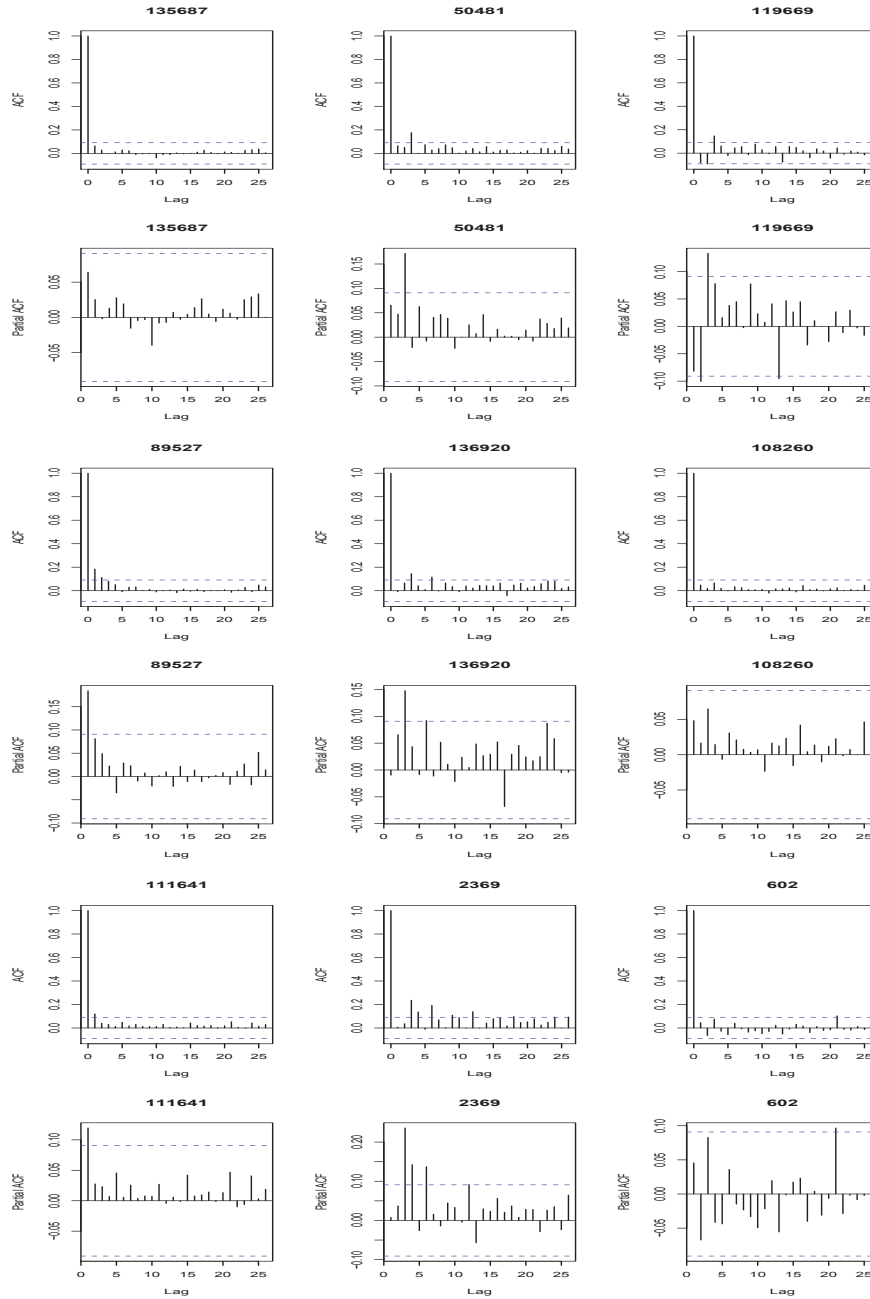


Figure 9: ACF and PACF plots for randomly selected voxels.

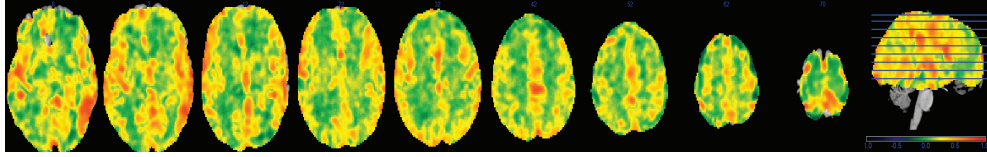


Figure 10: Estimates of ρ_v for each voxel.

positives. Overall, the use of an AR(1) temporal dependence seems quite reasonable in this example.

5 Discussion

We have developed a Bayesian hierarchical model which incorporates both spatial and temporal correlation. In the process we demonstrated how to incorporate a time-varying coefficient that allows for the variety of processes that might impact a BOLD response to a task during scanning. This work has the potential to have a broad and immediate impact on single-subject and -session fMRI task activation studies, which are the common first step when performing an fMRI study. Moreover, recent developments in the clinical usage of fMRI rely on subject- and session-specific investigations to locate and investigate language areas prior to brain surgery (Sabsevitz et al. 2003). In addition, for diseases such as AD, it is hoped that imaging can be used as a diagnostic utility for initiating treatment (Bassett et al. 2006).

For broader goals it would be of interest to extend the model to group studies. One approach would be to mirror existing group studies and adopt a two-stage frequentist/least squares approach (see Friston et al. 2007). That is, use posterior quantities from the subject-specific models in standard second-stage inter-subject regression models. A more satisfying answer would incorporate recent developments in fMRI meta-analysis models (Kang et al. 2011), employing a Bayesian second-stage model. Yet another alternative would build a global Bayesian model for groups of whole brain functional images, without relying on two-stage methods. However, such a solution presents numerous modeling and computational challenges. For example, the study of MCMC convergence in such high dimensional settings remains unexplored (present study included). Hence the consequences of having far more parameters than possible MCMC iterations remains unknown. Moreover, any fully Bayesian model for groups must not require loading the full inter-subject data set into memory to be scalable to the ever-increasing scope of fMRI studies. For many of these problems variational Bayesian solutions may be important future directions.

Despite computational and modeling difficulties, we are confident that Bayesian approaches represent an important direction in fMRI, and high-dimensional research in general. Studies such as the present one and others (e.g. Smith and Fahrmeir 2007; Caffo et al. 2011; Bowman et al. 2008; Goldsmith et al. 2014) demonstrate the practicality, efficacy and feasibility of general Bayesian solutions to these problems.

References

- Aguirre, G. K., Zarahn, E., and D'Esposito, M. (1997). "Empirical analyses of BOLD fMRI statistics. II. Spatially smoothed data collected under null-hypothesis and experimental conditions." *NeuroImage*, 5: 199–212. [700](#)
- Bassett, S. S., Yousem, D. M., Cristinzio¹, C., Kusevic¹, I., Yassa¹, M. A., Caffo, B. S., and Zeger, S. L. (2006). "Familial risk for Alzheimer's disease alters fMRI activation patterns." *Brain*, 129: 1229–1239. [724](#)
- Bench, C. J., Frith, C. D., Grasby, P. M., Friston, K. J., Paulesu, E., Frackowiak, R. S. J., , and Dolan, R. J. (1993). "Investigations of the functional anatomy of attention using the Stroop test." *Neuropsychologia*, 31: 907–922. [702](#)
- Bowman, F., Caffo, B., Bassett, S., and Kilts, C. (2008). "A Bayesian hierarchical framework for spatial modeling of fMRI data." *NeuroImage*, 39: 146–156. [700](#), [724](#)
- Caffo, B., Bowman, F., Eberly, L., and Bassett, S. (2011). "A Markov chain Monte Carlo based analysis of a multilevel model for functional MRI data." In Brooks, S., Gelman, A., Jones, G., and Meng, X.-L. (eds.), *Handbook of Markov Chain Monte Carlo*. Boca Raton, FL: CRC Press. [700](#), [724](#)
- Carter, C. S., Mintum, M., and Cohen, J. D. (1995). "Interference and facilitation effects during selective attention: H₂¹⁵O study of Stroop task performance." *NeuroImage*, 280: 747–749. [702](#)
- Chen, S., Wang, C., Eberly, L., Caffo, B., and Schwartz, B. (2009). "Adaptive control of the false discovery rate in voxel-based morphometry." *Human Brain Mapping*, 30: 2304–2311. [700](#)
- Davidson, D. J., Zacks, R. T., and Williams, C. C. (2003). "Stroop interference, practice, and aging." *Neuropsychology*, 10: 85–98. [702](#)
- Fernández, C., Ley, E., and Steel, M. F. J. (2001). "Benchmark priors for Bayesian model averaging." *Journal of Econometrics*, 100: 381–427. [703](#)
- Fisher, L. M., Freed, D. M., and Corkin, S. (1990). "Stroop color-word test performance in patients with Alzheimer's disease." *Journal of Clinical and Experimental Neuropsychology*, 12: 745–758. [702](#)
- Flegal, J. M. and Gong, L. (2013). "Relative fixed-width stopping rules for Markov chain Monte Carlo simulations." *arXiv:1303.0238*. [708](#)
- Flegal, J. M., Haran, M., and Jones, G. L. (2008). "Markov chain Monte Carlo: Can we trust the third significant figure?" *Statistical Science*, 23: 250–260. [708](#)
- Flegal, J. M. and Jones, G. L. (2011). "Implementing Markov chain Monte Carlo: estimating with confidence." In Brooks, S., Gelman, A., Jones, G., and Meng, X.-L. (eds.), *Handbook of Markov Chain Monte Carlo*. Boca Raton, FL: CRC Press. [708](#)

- Friston, K. J., Ashburner, J. T., Kiebel, S. J., Nichols, T. E., and Penny, W. D. (2007). *Statistical parametric mapping: The analysis of functional brain images*. Elsevier/Academic Press. 702, 703, 724
- Friston, K. J., Fletcher, P., Josephs, O., Holmes, A., Rugg, M., and Turner, R. (1998). “Event-related fMRI: characterizing differential responses.” *Neuroimage*, 7: 30–40. 700
- Friston, K. J., Holmes, A., Worsley, K. J., Polin, J. B., Frith, C., and Frackowiak, R. (1995). “Statistical parametric maps in functional imaging: A general linear approach.” *Human Brain Mapping*, 2: 189–210. 704
- Friston, K. J., Worsley, K., Frackowiak, R., Mazziotta, J., and Evans, A. (1994). “Assessing the significance of focal activations using their spatial extent.” *Human Brain Mapping*, 1: 210–220. 700
- Gelman, A. (1998). “Simulating normalizing constants: From importance sampling to bridge sampling to path sampling.” *Statistical Science*, 13: 163–185. 711
- Genovese, C. (2000). “A Bayesian time-course model for functional magnetic resonance imaging data.” *Journal of the American Statistical Association*, 95: 691–703. 700, 704
- George, E. I. (2000). “The variable selection problem.” *Journal of the American Statistical Association*, 95: 1304–1308. 703
- George, E. I. and McCulloch, R. E. (1993). “Variable selection via Gibbs sampling.” *Journal of the American Statistical Association*, 88: 881–889. 700
- (1997). “Approaches for Bayesian variable selection.” *Statistica Sinica*, 7: 339–374. 700
- Glover, G. H. (1999). “Deconvolution of impulse response in event-related BOLD.” *NeuroImage*, 9: 416–429. 700
- Goldsmith, J., Huang, L., and Crainiceanu, C. M. (2014). “Smooth scalar-on-image regression via spatial Bayesian variable selection.” *Journal of Computational and Graphical Statistics*, 23: 46–64. 700, 724
- Gössl, C., Fahrmeir, L., and Auer, D. P. (2001). “Bayesian spatiotemporal inference in functional magnetic resonance images.” *Biometric*, 57: 554–562. 700
- Johnson, A. A., Jones, G. L., and Neath, R. C. (2013). “Component-wise Markov chain Monte Carlo: Uniform and geometric ergodicity under mixing and composition.” *Statistical Science*, 28: 360–375. 708
- Jones, G. L., Haran, M., Caffo, B. S., and Neath, R. (2006). “Fixed-width output analysis for Markov chain Monte Carlo.” *Journal of the American Statistical Association*, 101: 1537–1547. 708, 717, 719

- Kang, J., Johnson, T. D., Nichols, T. E., and Wager, T. D. (2011). “Meta analysis of functional neuroimaging data via Bayesian spatial point processes.” *Journal of the American Statistical Association*, 106: 124–134. [724](#)
- Lee, K.-J. (2010). “Computational issues in using Bayesian hierarchical methods for the spatial modeling of fMRI data.” Ph.D. thesis, University of Minnesota, School of Statistics. [701](#), [704](#)
- Li, C., Zheng, J., Wang, J., Gui, L., and Li, C. (2009). “An fMRI Stroop task study of prefrontal cortical function in normal aging, mild cognitive impairment, and Alzheimer’s disease.” *Current Alzheimer Research*, 6: 525–530. [702](#)
- Liang, F., Paulo, R., Molina, G., Clyde, M. A., and Berger, J. O. (2008). “Mixture of g-priors for Bayesian variable selection.” *Journal of the American Statistical Association*, 410–423. [703](#)
- Lindquist, M. A. (2008). “The statistical analysis of fMRI data.” *Human Brain Mapping*, 23: 439–464. [700](#)
- Lindquist, M. A., Loh, J. M., Atlas, L. Y., and Wager, T. D. (2009). “Modeling the hemodynamic response function in fMRI: Efficiency, bias and mis-modeling.” *NeuroImage*, 45: S187–198. [703](#), [704](#)
- Locascio, J., Jennings, P. J., Moore, C. I., and Corkin, S. (1997). “Time series analysis in the time domain and resampling methods for studies of functional magnetic brain imaging.” *Human Brain Mapping*, 5: 168–193. [704](#)
- Lund, T. E., Madsen, K. H., Sidaros, K., Luo, W. L., and Nichols, T. E. (2006). “Non-white noise in fMRI: Does modelling have an impact?” *NeuroImage*, 29: 54–66. [703](#)
- Møller, J. (2003). *Spatial Statistics and Computational Methods*. Springer. [707](#)
- Nichols, T. and Holmes, A. (2002). “Nonparametric permutation tests for functional neuroimaging: A primer with examples.” *Human Brain Mapping*, 15: 1–25. [700](#)
- Polk, T., Drake, R., Jonides, J., Smith, M., and Smith, E. (2008). “Attention enhances the neural processing of relevant features and suppresses the processing of irrelevant features in humans: A functional magnetic resonance imaging study of the Stroop task.” *The Journal of Neuroscience*, 28: 13786–13792. [702](#)
- Propp, J. G. and Wilson, D. B. (1996). “Exact sampling with coupled Markov chains and applications to statistical mechanics.” *Random Structures and Algorithms*, 9: 223–252. [712](#)
- Raftery, A. (1996). “Hypothesis testing and model selection.” In Gilks, W., Richardson, S., and Spiegelhalter, D. (eds.), *Markov Chain Monte Carlo in Practice*. London: Chapman & Hall. [708](#)

- Rajapakse, J. C., Kruggel, F., Maisog, J. M., and Cramon, D. Y. (1998). “Modeling hemodynamic response for analysis of functional MRI time-series.” *Human Brain Mapping*, 6: 283–300. 703
- Sabsevitz, D. S., Swanson, S. J., Hammeke, T. A., Spanaki, M. V., Possing, E. T., Morris, G. L., Mueller, W. M., and Binder, J. R. (2003). “Use of preoperative functional neuroimaging to predict language deficits from epilepsy surgery.” *Neurology*, 60: 1788. 724
- Smith, M. and Fahrmeir, L. (2007). “Spatial Bayesian variable selection with application to functional magnetic resonance imaging.” *Journal of the American Statistical Association*, 102: 417–431. 700, 701, 704, 706, 708, 724
- Smith, M., Pütz, B., Auer, D., and Fahrmeir, L. (2003). “Assessing brain activity through spatial Bayesian variable selection.” *NeuroImage*, 20: 802–815. 700, 701, 704
- Stroop, J. R. (1935). “Studies of interference in serial verbal reactions.” *Journal of Experimental Psychology*, 7: 643–661. 701
- Taylor, S. F., Kornblum, S., Lauber, E. J., Minoshima, S., and Koeppe, R. A. (1997). “Isolation of specific interference processing in the Stroop task: PET activation studies.” *NeuroImage*, 6: 81–92. 702
- Tjelmeland, H. and Besag, J. (1998). “Markov random fields with higher-order interactions.” *Scandinavian Journal of Statistics*, 25: 415–433. 705
- Wang, F. and Landau, D. (2001). “Efficient, multiple-range random walk algorithm to calculate the density of states.” *Physical Review Letters*, 81: 2050 – 2053. 711
- Woolrich, M. W., Jenkinson, M., Brady, J. M., and Smith, S. M. (2004). “Fully Bayesian spatio-temporal modeling for fMRI data.” *IEEE Transactions on Medical Imaging*, 23: 213–231. 700
- Woolrich, M. W., Ripley, B. D., Brady, M., and Smith, S. M. (2001). “Temporal autocorrelation in univariate linear modeling of fMRI Data.” *NeuroImage*, 14: 1370–1386. 703
- Worsley, K. (2003). “Detecting activation in fMRI data.” *Statistical Methods in Medical Research*, 12: 401–418. 700
- Worsley, K., Marrett, S., Neelin, P., and Evans, A. (1992). “A three-dimensional statistical analysis for CBF activation studies in human brain.” *Journal of Cerebral Blood Flow and Metabolism*, 12: 900–918. 700
- Worsley, K. J., Liao, C. H., Aston, J., Petre, V., Duncan, G. H., Morales, F., and Evans, A. C. (2002). “A general statistical analysis for fMRI data.” *NeuroImage*, 15: 1–15. 703

- Xia, J., Liang, F., and Wang, Y. M. (2009). “fMRI analysis through Bayesian variable selection with a spatial prior.” *IEEE International Symposium on Biomedical Imaging (ISBI)*, 714–717. 700, 704
- Zellner, A. (1996). “On assessing prior distributions and Bayesian regression analysis with g -prior distributions.” In *Bayesian Inference and Decision Techniques: Essays in Honor of Brunode Finetti North-Holland/Elsevier*, 233–243. 703
- Zhang, C. and Ma, J. (2007). “Simulation via direct computation of partition functions.” *Physical Review Letters E*, 76: 036708–1–5. 711

Acknowledgments

Lee was supported by the National Science Foundation. Jones was supported by the National Science Foundation and the National Institutes for Health. Jones was also provided support by CRiSM during a visit to the University of Warwick. Caffo was supported by the National Institutes for Health.

Appendix: Derivation of $q(\gamma, \rho, \theta|y)$

$$\begin{aligned}
q(\gamma, \rho, \theta|y) &\propto \int q(\beta(\gamma), \gamma, \rho, \theta, \sigma^2|y) d\beta(\gamma) d\sigma^2 \\
&\propto \pi(\gamma|\theta)\pi(\rho)\pi(\theta) \\
&\quad \times \prod_{v=1}^N \int p(y_v|\beta_v(\gamma_v), \gamma_v, \sigma_v^2, \Lambda_v)\pi(\beta_v(\gamma_v)|y_v, \gamma_v, \sigma_v^2, \Lambda_v)\pi(\sigma_v^2) d\beta_v(\gamma_v) d\sigma_v^2.
\end{aligned}$$

Consider the integrand

$$\begin{aligned}
&p(y_v|\beta_v(\gamma_v), \gamma_v, \sigma_v^2, \Lambda_v)\pi(\beta_v(\gamma_v)|y_v, \gamma_v, \sigma_v^2, \Lambda_v)\pi(\sigma_v^2) \\
&\propto \left[\frac{|(1/T_v)X_v^T(\gamma_v)\Lambda_v^{-1}X_v(\gamma_v)|}{|\Lambda_v|} \right]^{1/2} \\
&\quad \times \exp \left\{ -\frac{1}{2\sigma_v^2} [(y_v - X_v(\gamma_v)\beta_v(\gamma_v))^T \Lambda_v^{-1}(y_v - X_v(\gamma_v)\beta_v(\gamma_v)) \right. \\
&\quad \left. + \frac{1}{T_v} (\beta_v(\gamma_v) - \hat{\beta}_v(\gamma_v))^T X_v^T(\gamma_v)\Lambda_v^{-1}X_v(\gamma_v)(\beta_v(\gamma_v) - \hat{\beta}_v(\gamma_v))] \right\} \\
&\quad \times (\sigma_v^2)^{-(1+(T_v+q_v)/2)} (2\pi)^{-q_v/2} \\
&= \left[\frac{|(1/T_v)X_v^T(\gamma_v)\Lambda_v^{-1}X_v(\gamma_v)|}{|\Lambda_v|} \right]^{1/2} (\sigma_v^2)^{-(1+(T_v+q_v)/2)} (2\pi)^{-q_v/2} \times \\
&\quad \times \exp \left\{ -\frac{1 + \frac{1}{T_v}}{2\sigma_v^2} [\beta_v^T(\gamma_v)X_v^T(\gamma_v)\Lambda_v^{-1}X_v(\gamma_v)\beta_v(\gamma_v) - 2y_v^T \Lambda_v^{-1}X_v(\gamma_v)\beta_v(\gamma_v)] \right\} \\
&\quad \times \exp \left\{ -\frac{1}{2\sigma_v^2} y_v^T \left[\Lambda_v^{-1} + \frac{1}{T_v} \Lambda_v^{-1}X_v(\gamma_v) (X_v^T(\gamma_v)\Lambda_v^{-1}X_v(\gamma_v))^{-1} X_v^T(\gamma_v)\Lambda_v^{-1} \right] y_v \right\}.
\end{aligned}$$

Now let $A_v = X_v^T \Lambda_v^{-1} X_v(\gamma_v)$ and $C_v = y_v^T \Lambda_v^{-1} X_v(\gamma_v)$. Note that

$$(\beta_v(\gamma_v) - A_v^{-1}C_v^T)^T A(\beta_v(\gamma_v) - A_v^{-1}C_v^T) - C_v A_v^{-1}C_v^T = \beta_v^T(\gamma_v)A_v\beta_v(\gamma_v) - 2C_v\beta_v(\gamma_v).$$

Hence

$$\begin{aligned}
&p(y_v|\beta_v(\gamma_v), \gamma_v, \sigma_v^2, \Lambda_v)\pi(\beta_v(\gamma_v)|y_v, \gamma_v, \sigma_v^2, \Lambda_v)\pi(\sigma_v^2) \\
&\propto \left[\frac{|X_v^T(\gamma_v)\Lambda_v^{-1}X_v(\gamma_v)|}{|\Lambda_v|} \right]^{1/2} (\sigma_v^2)^{-(1+(T_v+q_v)/2)} (2\pi T_v)^{-q_v/2} \times \\
&\quad \times \exp \left\{ -\frac{1}{2\sigma_v^2} \left(1 + \frac{1}{T_v} \right) (\beta_v(\gamma_v) - A_v^{-1}C_v^T)^T A(\beta_v(\gamma_v) - A_v^{-1}C_v^T) \right\} \times \\
&\quad \times \exp \left\{ -\frac{1}{2\sigma_v^2} y_v^T \left[\Lambda_v^{-1} - \Lambda_v^{-1}X_v(\gamma_v) (X_v^T(\gamma_v)\Lambda_v^{-1}X_v(\gamma_v))^{-1} X_v^T(\gamma_v)\Lambda_v^{-1} \right] y_v \right\}.
\end{aligned}$$

Now

$$\begin{aligned}
 & q(\gamma, \theta, \rho | y) \\
 & \propto \pi(\gamma | \theta) \pi(\rho) \pi(\theta) \prod_{v=1}^N \left[\frac{|X_v^T(\gamma_v) \Lambda_v^{-1} X_v(\gamma_v)|}{|\Lambda_v|} \right]^{1/2} (2\pi T_v)^{-q_v/2} \times \int \frac{1}{(\sigma_v^2)^{1+\frac{T_v+q_v}{2}}} \\
 & \quad \times \exp \left\{ -\frac{1}{2\sigma_v^2} y_v^T \left[\Lambda_v^{-1} - \Lambda_v^{-1} X_v(\gamma_v) (X_v^T(\gamma_v) \Lambda_v^{-1} X_v(\gamma_v))^{-1} X_v^T(\gamma_v) \Lambda_v^{-1} \right] y_v \right\} \\
 & \quad \times \int \exp \left\{ -\frac{1}{2\sigma_v^2} \left(1 + \frac{1}{T_v} \right) (\beta_v(\gamma_v) - A_v^{-1} C_v^T)^T A (\beta_v(\gamma_v) - A_v^{-1} C_v^T) \right\} d\beta_v(\gamma_v) d\sigma_v^2 \\
 & = \pi(\gamma | \theta) \pi(\rho) \pi(\theta) \prod_{v=1}^N \frac{1}{(1+T_v)^{q_v/2} |\Lambda_v|^{1/2}} \left[\int \frac{1}{(\sigma_v^2)^{1+\frac{T_v}{2}}} \right. \\
 & \quad \left. \times \exp \left\{ -\frac{1}{2\sigma_v^2} y_v^T \left[\Lambda_v^{-1} - \Lambda_v^{-1} X_v(\gamma_v) (X_v^T(\gamma_v) \Lambda_v^{-1} X_v(\gamma_v))^{-1} X_v^T(\gamma_v) \Lambda_v^{-1} \right] y_v \right\} \right] d\sigma_v^2 \\
 & \propto \pi(\gamma | \theta) \pi(\rho) \pi(\theta) \prod_{v=1}^N \left[\frac{1}{(1+T_v)^{q_v/2} |\Lambda_v|^{1/2}} \right. \\
 & \quad \left. \times \left(y_v^T \left[\Lambda_v^{-1} - \Lambda_v^{-1} X_v(\gamma_v) (X_v^T(\gamma_v) \Lambda_v^{-1} X_v(\gamma_v))^{-1} X_v^T(\gamma_v) \Lambda_v^{-1} \right] y_v \right)^{-T_v/2} \right] \\
 & = \pi(\gamma | \theta) \pi(\rho) \pi(\theta) \prod_{v=1}^N \frac{1}{(1+T_v)^{q_v/2} |\Lambda_v|^{1/2}} S(\rho_v, \gamma_v)^{-T_v/2}.
 \end{aligned}$$

